Exp Fluids (2014) 55:1653
DOI 10.1007/s00348-013-1653-9

RESEARCH ARTICLE

# Mesler entrainment in alcohols

**R. K. Sundberg-Anderson · J. R. Saylor**

Received: 5 March 2013 / Revised: 7 November 2013 / Accepted: 14 December 2013 / Published online: 5 January 2014


**Abstract** Mesler entrainment has been studied extensively in water and, more recently, in silicone oils. Studies of Mesler entrainment in liquids other than these are rare. The extant experimental results in water show significant irreproducibility both in the qualitative characteristics of Mesler entrainment and in the existence or nonexistence of Mesler entrainment when, for example, drops of the same diameter are released from the same height. In contrast, in silicone oils, Mesler entrainment is highly reproducible, essentially occurring either all of the time, or none of the time for a given set of conditions. A goal of the present work was to determine which of these two behaviors is the "standard" behavior—that is, to determine whether Mesler entrainment is typically repeatable or not. The experimental studies presented herein were conducted in three liquids that have not been the subject of detailed investigation to date: ethyl alcohol, isopropyl alcohol, and methyl alcohol. All of these alcohol results showed behavior very similar to that observed in silicone oils, suggesting that Mesler entrainment is typically repeatable and that water is an atypical fluid, causing irreproducible results. Additionally, we present data obtained in silicone oils and combine that with the alcohol data in an attempt to develop a combination of dimensionless groups that predicts the boundaries within which Mesler entrainment occurs for liquids other than water.

R. K. Sundberg-Anderson · J. R. Saylor (✉)
Clemson University, Clemson, SC, USA
e-mail: jsaylor@clemson.edu

R. K. Sundberg-Anderson
e-mail: rsundbe@clemson.edu

## 1 Introduction

When a liquid drop impacts a flat, quiescent surface of the same liquid, a thin film of air becomes temporarily trapped between the drop and the bulk liquid. At small impact, velocities, typically achieved by releasing a drop from a relatively low height, drops float or bounce on the bulk liquid surface before the air film drains away and the drop coalesces with the bulk. At larger impact, velocities, the air film caught between the drop and the bulk interfaces, can break up during coalescence, resulting in the formation of one or more bubbles depending on the conditions of the impact. Mesler entrainment is one type of bubble formation that can occur when the air film breaks down. This type of bubble formation occurs for a specific range of drop impact conditions, resulting in a large number of very small bubbles. This phenomenon was first noted by Russell Mesler during his studies on nucleate boiling (Bergman and Mesler 1981; Mesler 1976; Mesler and Mailen 1977), where he observed the entrainment of hundreds of micron scale bubbles often displaying a chandelier-like pattern following the impact of a water drop with a bulk water surface (Carroll and Mesler 1981).

Mesler's original work focused on boiling, specifically on his observation that new nucleation sites tended to form near existing ones. Mesler postulated that bubbles released during boiling rose and subsequently popped at the air/liquid interface, forming small drops that would fall back to the air/liquid interface and entrain air bubbles that would propagate back down to the solid surface via a vortex, thereby spawning new nucleation sites there (Bergman and Mesler 1981; Carroll and Mesler 1981; Mesler and Mailen 1977). This research amplified interest in drop impact phenomena in general and Mesler entrainment in particular. There have been several studies of Mesler entrainment

(Bergman and Mesler 1981; Carroll and Mesler 1981; Esmailizadeh and Mesler1986; Liow and Cole 2007; Mesler 1976; Mesler and Mailen 1977; Oğuz and Prosperetti 1989; Pumphrey and Elmore 1990; Sigler and Mesler 1990, Thoroddsen et al. 2003, 2012), and good surveys of the extant work can be found in Saylor and Bounds (2012) and Mills et al. (2012). More recent research on Mesler entrainment has been motivated by environmental applications such as the enhanced gas exchange that may occur due to Mesler entrainment beneath small drops formed by, for example, splash drops formed by raindrop impacts, bubbles popping at the water surface, and by small drops formed by breaking waves (Mills et al. 2012; Saylor and Bounds 2012).

Until recently, Mesler entrainment was characterized as having an unpredictable nature, in that it did not show reproducibility. This was true, for example, of the work due to Esmailizadeh and Mesler (1986), Sigler and Mesler (1990), and Pumphrey and Elmore (1990). The lack of reproducibility was often attributed to the presence of contaminants on the liquid surface (Esmailizadeh and Mesler 1986; Sigler and Mesler 1990). Mills et al. (2012) noted that at the time of their study, almost all of the prior work on Mesler entrainment had used water as the working fluid, which is highly susceptible to adventitious surfactants. They suggested that these adventitious surfactants could be the contaminants that caused irreproducibility. To explore this possibility, these authors purposely contaminated their water with a soluble surfactant in an attempt to overwhelm any contaminating surfactants and thereby improve the reproducibility. However these studies did not result in improved reproducibility, leaving unanswered the question of exactly why Mesler entrainment is not reproducible in water.

Saylor and Bounds showed that reproducible Mesler entrainment could be obtained using silicone oil, as opposed to water (Saylor and Bounds 2012). They presented the first detailed studies of Mesler entrainment in liquids other than water, using two silicone oils having different viscosities, and showed highly reproducible behavior for both. Part of their results is reproduced in Fig. 1 which is a plot of $f$ versus $We$ for the two silicone oils and water. Here, $f$ is the fraction of the time that Mesler entrainment occurs for a given set of trials, and $We$ is the Weber number (defined below). The figure shows that for both of the silicone oils investigated, $f$ was either zero or one with almost no exceptions, indicating that Mesler entrainment occurred all of the time or none of the time. Water, on the other hand, shows a range of values for $f$ and never attained a value of $f$ greater than 0.8.

Figure 1 shows that Mesler entrainment is highly repeatable for silicone oils and not very repeatable for water. Although this suggests that a more fruitful path for

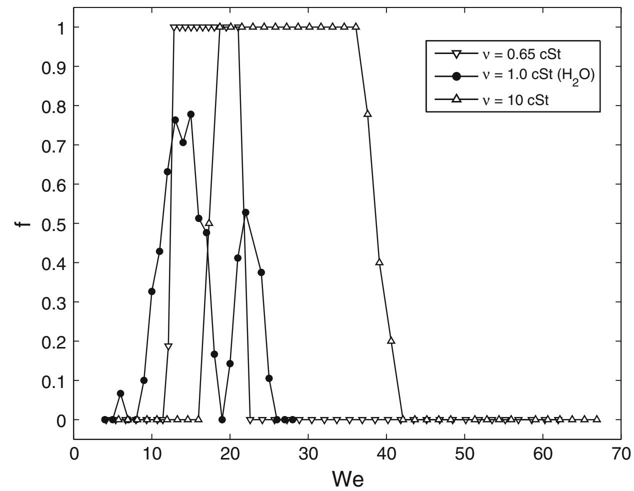


**Fig. 1** Plot of frequency of occurrence of Mesler entrainment $f$ versus Weber number $We$ for two silicone oils and water. The kinematic viscosity ν is included in the legend for each of the three liquids. Figure taken from Saylor and Bounds (2012)

research in Mesler entrainment will most likely be found using silicone oils, the results presented in Fig. 1 do not reveal which of these two behaviors is the "standard" behavior. That is, it is not clear whether most liquids will display repeatable behavior like silicone oils, or non-repeatable behavior like water. To address this question, experiments are presented herein using three other liquids: isopropyl alcohol, methyl alcohol, and ethyl alcohol.

We note in passing that there is one earlier study wherein alcohols were investigated, this being the work of Esmailizadeh and Mesler, where 1-butanol, n-amyl alcohol, methyl alcohol, and isopropyl alcohol were investigated (Esmailizadeh and Mesler 1986). This was a photographic study, but photographs were not actually presented for any of these liquids. Moreover, the authors only noted that in these liquids, there were fewer bubbles than for the other liquids studied and that these bubbles were smaller.

Recent developments in high-speed camera technology have enabled time-resolved visualizations of Mesler entrainment. Especially notable in this regard is the work by Thoroddsen and co-workers who have presented highly resolved details of how the air film collapses in the process of forming Mesler bubbles (Thoroddsen et al. 2003, 2012). These authors show, for example, that the air film can collapse in one or more locations initially, after which the collapse propagates azimuthally around the crater, and how this affects the resulting bubble pattern. These authors also suggest that just prior to collapse, this air film tends to be on the order of 100 nm, at least for the parameter space that they explored. In spite of these dramatic improvements in visualization, as well as the relatively large body of work on Mesler entrainment overall, the mechanism that causes the air film to collapse during Mesler entrainment is unknown. A first step in this direction is determining the correct combination of dimensionless groups that define the boundaries within which Mesler entrainment occurs.

Assuming that the relevant parameters for bubble formation by drop impacts are the drop diameter $D$, impact velocity $V$, liquid density $\rho$, liquid dynamic viscosity $\mu$, and surface tension $\sigma$ as well as the acceleration due to gravity $g$, the resulting dimensionless groups are the Weber, Froude, and capillary numbers, defined as:

$$We = \frac{\rho D V^2}{\sigma} \quad (1)$$

$$Fr = \frac{V^2}{gD} \quad (2)$$

$$Ca = \frac{\mu V}{\sigma} \quad (3)$$

In the above development, the properties of the gas are ignored, which is appropriate so long as they do not vary, which is the case here where air is used at room temperature and pressure.

A useful step in the direction of determining the physical mechanism responsible for Mesler entrainment would be to determine the boundaries in ($We$, $Fr$, $Ca$) space within which Mesler entrainment occurs. Saylor and Bounds took a step in this direction in their study of silicone oils and water. In that work, they showed that the locations associated with the onset of Mesler entrainment (the left hand, or leading edges of the data in Fig. 1) collapse when plotted versus $We/Ca^{1/9}$, suggesting that $We$ dominates Mesler entrainment and that viscous effects are present, but of secondary importance. However, they did not show collapse for the trailing edge. Moreover, they used water and two silicone oils as their only data points, an approach which is probably questionable should it be the case that water displays very different behavior than other liquids (which we indeed show in this paper). Accordingly, the second goal of this paper is to obtain data for three more liquids and to use these in combination with silicone oil data in an attempt to determine the combination of ($We$, $Fr$, $Ca$) that predict the onset and/or end of Mesler entrainment.

## 2 Experimental method

Drop impact experiments were conducted using methyl alcohol, ethyl alcohol, and isopropyl alcohol. The overall approach employed in these experiments was to release drops from a range of heights for a given liquid. The fraction of drops that resulted in Mesler entrainment, $f$, was recorded at each height. By increasing the drop release height, the impact velocity increased which, along with the change in liquid properties resulting from the three different liquids used, as well as variations in drop diameter $D$, resulted in variation in ($We$, $Fr$, $Ca$). The properties of the liquids used here are presented in Table 1. The results of these experiments are initially plotted here on $f$ versus $We$ coordinates, since earlier work suggests that $We$ dominates the other parameters. Since variations in drop diameter were quite small for a given liquid (the standard deviation of the drop diameter was less than 1.1 % of the mean diameter for all liquids studied here), $We$ is a monotonic function of drop release height, for a given liquid. In all experiments, the drop and bulk fluids were identical.

**Table 1** CAS #, density, surface tension, and dynamic viscosity of the liquids investigated

| | CAS | $\rho$ (kg/m$^3$) | $\sigma$ (N/m) | $\mu$ (Pa·s) |
|---|---|---|---|---|
| Methyl alcohol | 67-56-1 | 787 | 0.0221 | $5.4 \times 10^{-4}$ |
| Ethyl alcohol | 64-17-5 | 785 | 0.022 | $1.07 \times 10^{-3}$ |
| Isopropyl alcohol | 67-63-0 | 781 | 0.0209 | $2.04 \times 10^{-3}$ |

All data taken at 25 °C (Weast 2012)

Because of the speed of the drop impact event and the small size of Mesler entrainment bubbles, it is not possible to determine whether Mesler entrainment has occurred via the unaided eye. Instead, some form of high-speed imaging is required. In these experiments this was done using two different setups which are shown in Figs. 2 and 3. The difference between these two setups exists primarily in the camera and lighting conditions. As will be described below, as the drop release height increased, the Mesler entrainment bubbles tended to get smaller, requiring different visualization capabilities for the high and low $We$ range.

In the first experimental setup, presented in Fig. 2, a high-speed camera (Cooke Scientific, pco.1200hs) was used to gather sequences of drop impact images over the Weber number range $3 < We < 15$. The camera is capable of nearly 1,000 frames per second and was fitted with a Canon 65 mm macro lens set to give 1X magnification. The camera had a 1,280 × 1,024 pixel array (although a subset of the entire region was often used), and a spatial resolution of 12 μm. Images were taken with back lighting from a white 8 × 16 LED array. The camera was positioned slightly below the bulk surface and pointed upward at an angle of approximately 4° so that bubble formation could be recorded unobstructed by the meniscus. Viewed in this way, the drop could not be seen due to total internal reflection beneath the bulk liquid surface. However, the time of drop impact was made obvious by the formation of a crater. Figure 4 shows a sequence of frames showing the

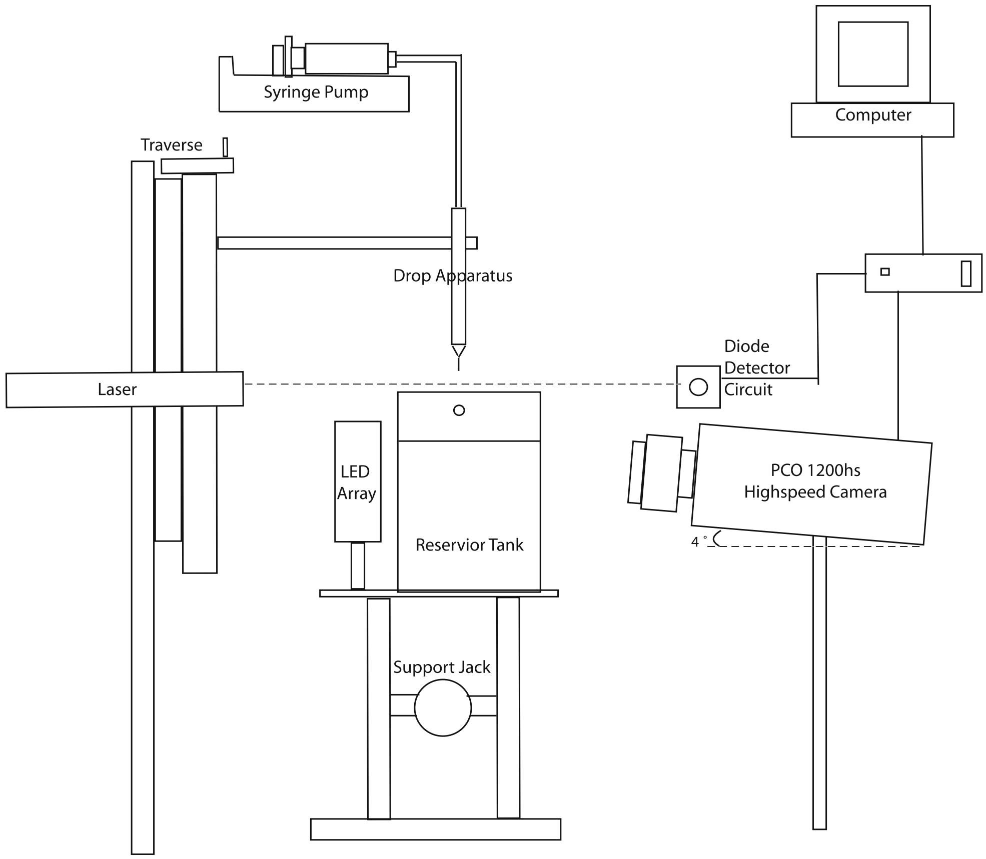


**Fig. 2** Experimental apparatus utilizing back lighting from an LED array for testing the low Weber number range

beginning of the crater formation, the crater just prior to bubble formation, the Mesler bubbles just as they are formed, and the Mesler bubbles after they have been transported into the bulk a short distance.

Image acquisition was initiated via a laser triggering circuit. As shown in Fig. 2, a HeNe laser was horizontally oriented just above the reservoir tank and directed at a photodiode located on the other side of the tank. The needle from which the drops emanated was located directly above the laser so that each drop interrupted the beam causing a step change in the diode voltage. The camera was operated in a mode where the image buffer was constantly overwritten, and the diode signal was used to trigger the camera to stop recording images after a set number of delay frames were taken, typically between 150 and 250. A subset of the acquired frames captured the impact of the drop and any subsequent events such as floating drops or bubble production. This subset of frames was analyzed to determine the value of $f$ at each drop release height.

At large drop release heights (large $We$), the entrained bubbles were smaller and could not be resolved using the setup shown in Fig. 2. This range of drop heights corresponded to Weber numbers greater than $\sim 15$. To address this problem, the setup shown in Fig. 3 was used, which differs from Fig. 2 primarily in that a larger format camera was used and the bubbles were illuminated via a strobe in a side lighting orientation (as opposed to continuous back illumination). A Canon DSLR camera (Rebel T3i, 18 megapixel) fitted with a Canon 65 mm macro lens was used at 3X magnification. The camera had a $5{,}184 \times 3{,}456$ pixel array, giving a spatial resolution of 1.45 µm/pixel, and was used to capture single images of Mesler entrainment as they were illuminated with a General Radio 1531-AB Strobotac. The strobe was located on one side of the bulk tank, nominally perpendicular to the camera, but angled slightly upward and toward the camera. The LED array, used for data collection in the low $We$ range, was removed and a sheet of black cloth was hung behind the tank to reduce reflection and glare. The entire apparatus was also placed inside a light-tight enclosure constructed of opaque plastic, virtually eliminating any ambient light and allowing the camera's shutter to remain open for extended periods of time without contributing significantly to the background light level in each image. The shutter speed was set to 15 s during which time, a single drop impact and strobe flash would occur.

The strobe was triggered by the same laser/photodiode combination as presented in Fig. 2. However in the strobe

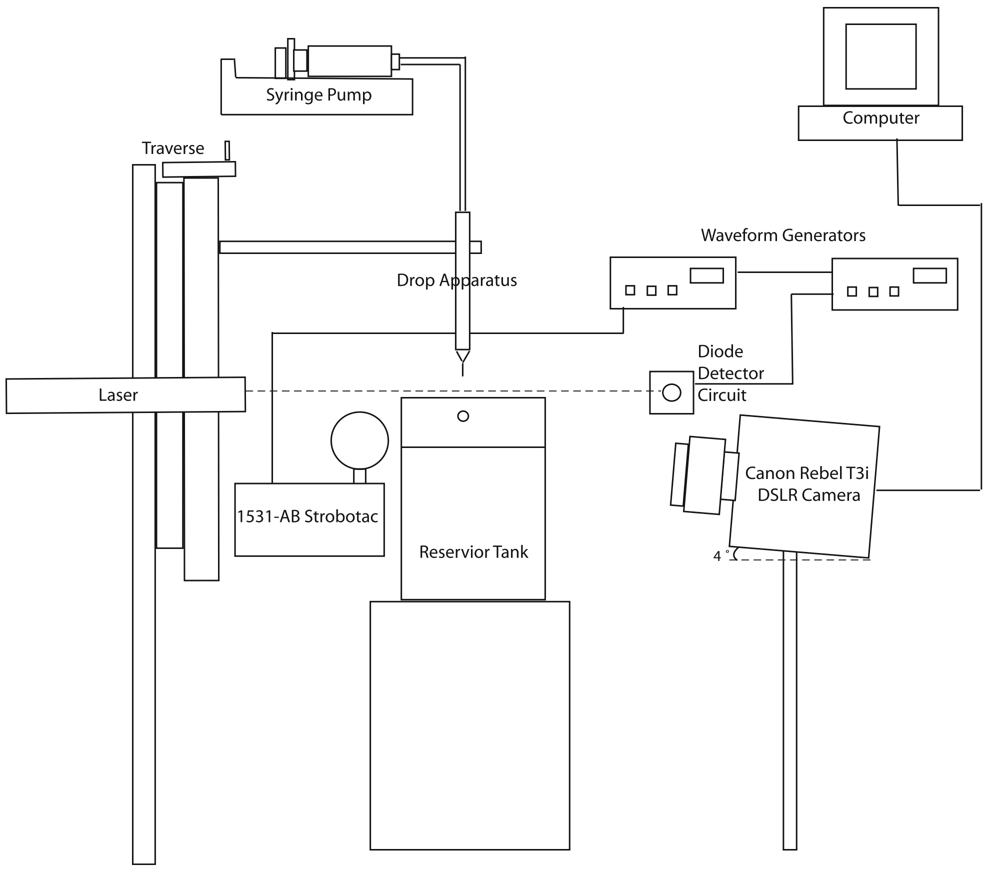


**Fig. 3** Experimental apparatus used for image acquisition at high Weber numbers

setup the photodiode signal generated when the drop fell through the beam was used to trigger a function generator (Agilent 33220A) which produced a single, variable width pulse. The trailing edge of this pulse triggered a second function generator (also an Agilent 33220A) which sent a square wave pulse that triggered the strobe. The timing of the strobe with respect to the laser trigger was controlled by the width of the pulse leaving the first function generator, enabling observation of any phase in the drop impact/bubble formation process.

A glass tank with interior dimensions of 3.5 × 3.5 × 7 inches was used for both experimental setups. The tank was filled and placed under a drop apparatus consisted of an 18-gauge needle fit to a length of plastic tubing, fastened to a vertical traverse. The drop release height was measured using a linear traverse having a resolution of 10 µm. Specifically, the water surface height was first determined by slowly lowering the needle until it pierced the liquid surface. This procedure was repeated five times in a row, and the average taken as the reference point from which the drop release height was measured. Because the liquid level was susceptible to slight changes due to evaporation, addition of drop fluid, and movement of the meniscus contact line, this process was repeated following every 2–3 drop release heights explored. This procedure was used in both experimental setups (those shown in Figs. 2, 3).

The spacing between nearly all drop release heights was 250 µm; however, on occasion a release height was skipped giving some data points at a larger spacing of 500 µm. This was done, for example, at large *We* once the trailing edge of the *f* versus *We* plot had been located. At that time, data points were acquired at progressively higher heights until evidence of drop splashing was noted.

A syringe pump delivered liquid through the tubing at a rate of 0.84 mL/h, resulting in a drop impact every 30 s. During the strobe experiments, a higher volumetric flowrate of 1.68 mL/h was used to give a drop every 15 s, permitting a shorter time during which the shutter had to be kept open.

For the multiple frame, backlit images obtained using the setup in Fig. 2, an entire sequence of about 200 frames was recorded for each drop impact. These sequences were stored and observed at the completion of the experiment to determine whether or not Mesler entrainment occurred. For these low Weber number runs, ten drops were released from each height explored. The corresponding value of *f* was determined by the ratio of the number of impacts resulting in Mesler entrainment to the total number of

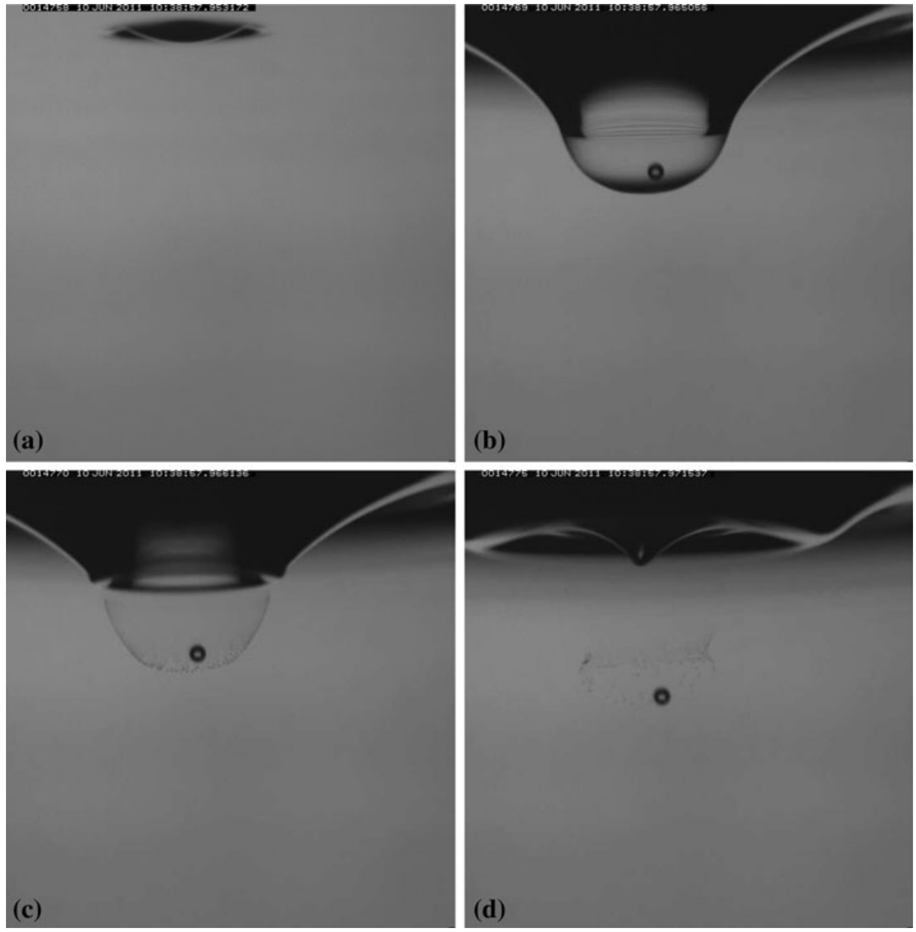


**Fig. 4** A sample image sequence showing Mesler entrainment in methyl alcohol ($We = 9.42$). **a** The beginning of the formation of the crater caused by the drop impacting the liquid surface (0 ms); **b** the crater is at its lowest depth—this is the point just prior to the formation of Mesler bubbles (11.88 ms); **c** the first frame when bubbles appear (12.96 ms); **d** the bubbles after they have been transported a short distance into the bulk (18.37 ms). Each frame is 6.4 mm in the horizontal direction and 6.5 mm in the vertical direction

drops released from the given height (ten). Each drop release height was tested in a randomized order so as to eliminate the possible effect of steady changes in environmental conditions.

For the single frame strobe images obtained using the setup in Fig. 3, a different approach was taken. Preliminary experiments revealed that even when Mesler entrainment was highly repeatable in terms of whether or not it occurred at a given drop release height, it was not very repeatable in terms of the exact moment in time when it occurred at a given drop release height. That is, at a fixed time delay between the laser trigger and the strobe flash, Mesler entrainment might not be observed, even though it had been observed for the same conditions earlier. Accordingly, the procedure for these experiments was to determine the time delay between the laser trigger and the strobe flash at which Mesler entrainment was nominally observed. Then, this time delay was increased slightly. In this way, while the exact moment of the formation of Mesler bubbles was sometimes missed, the bubbles themselves were not missed, since a relatively long period of time passes between the formation of the bubbles, and their convection out of the field of view. This insured that small variations in the time at which Mesler entrainment occurred still allowed for visualization of Mesler bubbles. After the appropriate time delay was determined, $\sim 5$ images were acquired at those settings. If all of these images resulted in Mesler entrainment, then that Weber number was assigned $f = 1$. It is noted that occasionally, after several drops had fallen, Mesler entrainment bubbles might not be visible, but would become visible again upon slight readjustment of the strobe position. In this case, those frames that showed no bubbles were not counted in computation of $f$. If no Mesler bubbles were noted despite recording images at multiple time delays, the corresponding Weber number was assigned $f = 0$.

Computation of each of the dimensionless groups defined in Eqs. (1)–(3) requires the drop impact velocity $V$ and the drop diameter $D$. These were measured by obtaining image sequences of drops falling prior to impact. These images were obtained using the pco.1200-hs high-speed camera, which was repositioned from the orientation shown in Fig. 2 so that it was located slightly above the bulk liquid surface and angled slightly downward. As the drop fell toward the bulk surface, 15–30 images were recorded prior to impact. These images were analyzed

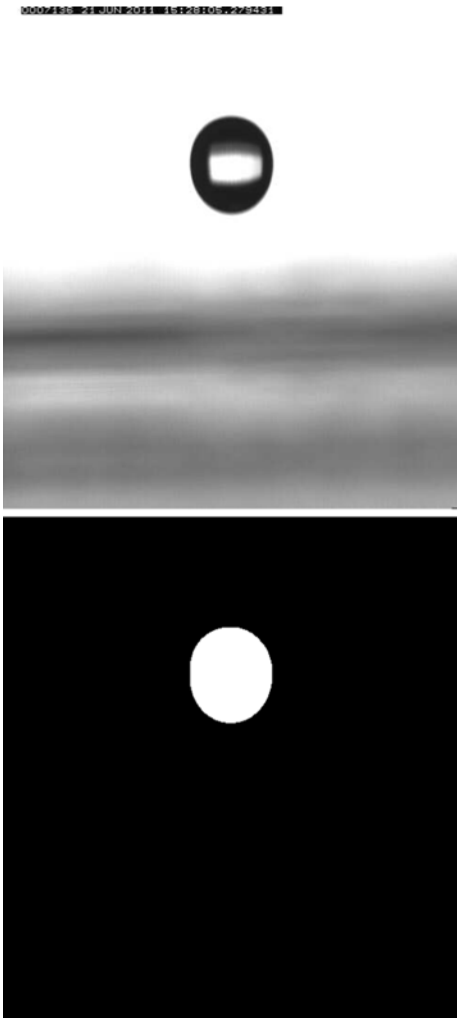

Fig. 5 Sample image of a falling drop imaged from above the liquid surface. These are for isopropyl alcohol drops released from a height of 18.0 mm ($We = 19.04$). The original *gray scale* image is on the top, and the processed image, obtained after edge detection and fill, is presented on the bottom. Each image is 12.67 mm wide and 13.96 mm tall

using the Canny (1986) edge detection algorithm to determine the outline of the drop in each frame. An example of the grayscale and processed version of a falling drop is presented in Fig. 5. The diameter of the drop was computed on a volume basis as the average of all the diameters in the image sequence assuming a drop that is circularly symmetric about its vertical axis. The drop centroid was computed for each image obtained in a sequence to determine its vertical position as a function of time. A linear fit to the position versus time data was performed for the final four frames in the sequence which displayed a drop prior to impact. A power law fit to the resulting velocity versus height data was performed using the form shown in Eq. (4):

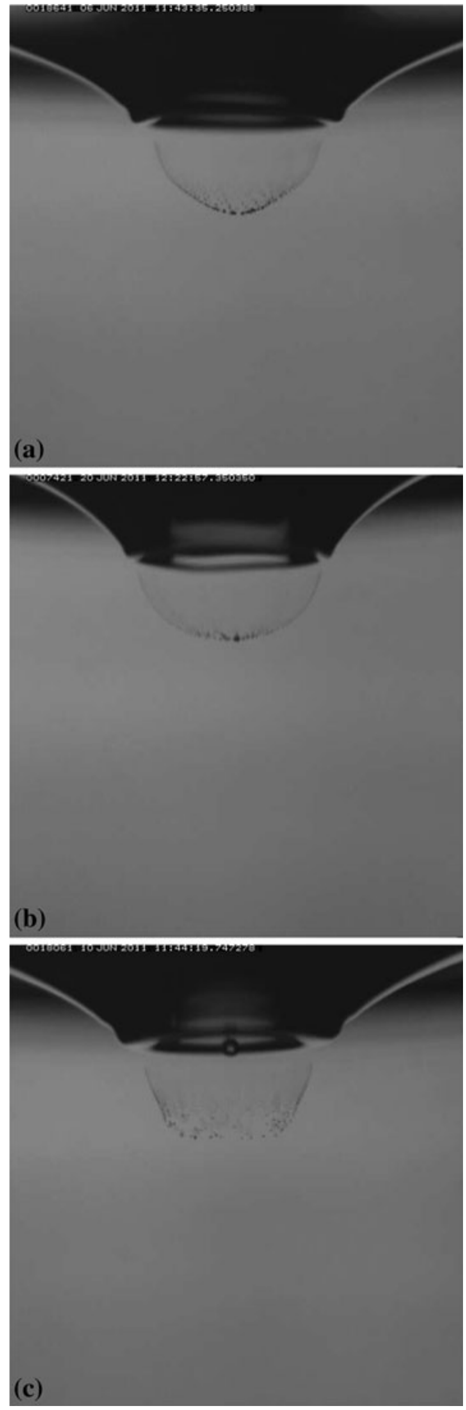


Fig. 6 Sample images of Mesler entrainment for the low Weber number range. Images are presented for **a** ethyl alcohol ($We = 9.83$), **b** isopropyl alcohol ($We = 15.0$), and **c** methyl alcohol ($We = 9.72$). These are backlit, and hence, the bubbles appear *black* on a *bright background*. Each image is 6.4 mm in the *horizontal* direction and 6.5 mm in the *vertical* direction

$$V = ah^b \tag{4}$$

where $h$ is the drop release height above the liquid surface, and $a$ and $b$ are parameters determined by a fit to the data.

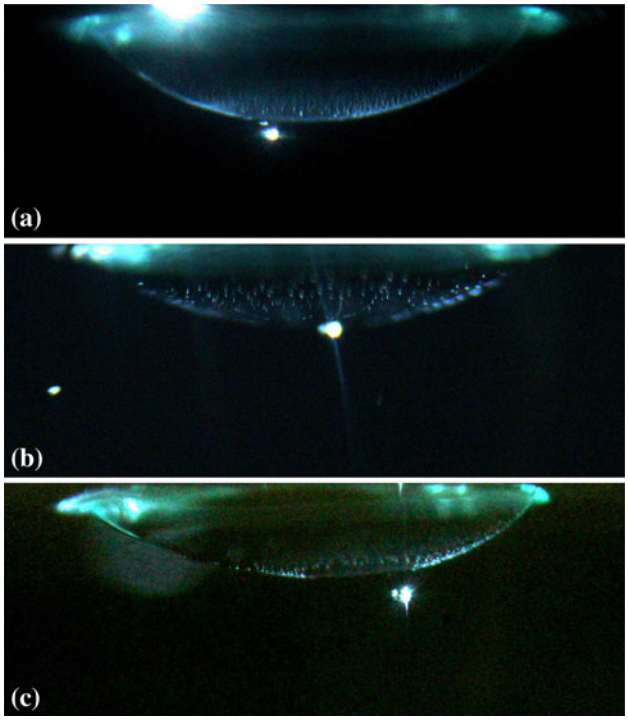


**Fig. 7** Sample images of Mesler entrainment for the high Weber number range. Images are presented for (**a**) ethyl alcohol ($We = 31.0$), **b** isopropyl alcohol ($We = 41.1$), and **c** methyl alcohol ($We = 20.2$). A strobe was used for illumination in these images, making the bubbles white on a black background. Each image is 4.48 mm in the horizontal direction and 1.69 mm in the vertical direction

This equation was used to calculate $V$ for use in Eqs. (1)–(3). This process was repeated for each liquid investigated.

## 3 Results

Sample images obtained for each of the three alcohols investigated herein are presented in Figs. 6 and 7 for the lower and upper ranges of $We$, respectively. A variety of bubble sizes and patterns were observed over the range of Weber numbers investigated, making classification of each entrainment event difficult. Because the mechanism that produces Mesler entrainment is not yet understood, there is no consensus as to the appropriate bubble size or pattern associated with Mesler entrainment. So, while the images presented in Figs. 6 and 7 are typical, other patterns were also observed. In this study, all impacts showing the production of at least ten small-scale bubbles were classified as Mesler entrainment.

Plots of $f$ versus $We$ are presented in Fig. 8 for methyl alcohol, ethyl alcohol, and isopropyl alcohol. To more clearly show the different data sets presented in Fig. 8, they are plotted separately in Figs. 9, 10 and 11. The overall

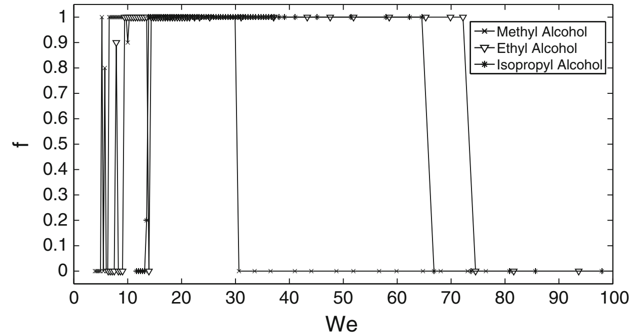


**Fig. 8** Plot of $f$ versus $We$ for ethyl alcohol, methyl alcohol, and isopropyl alcohol

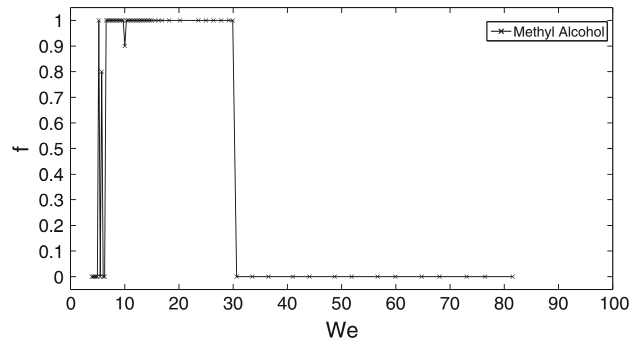


**Fig. 9** Plot of $f$ versus $We$ for methyl alcohol

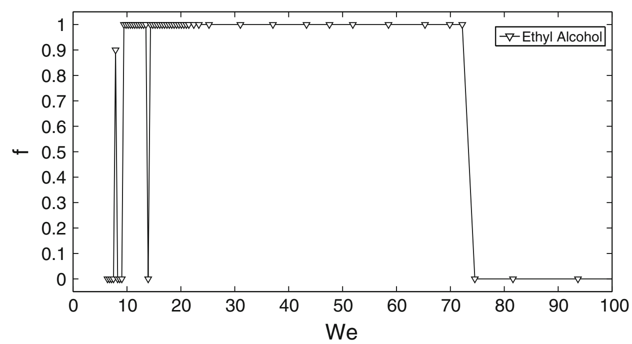


**Fig. 10** Plot of $f$ versus $We$ for ethyl alcohol

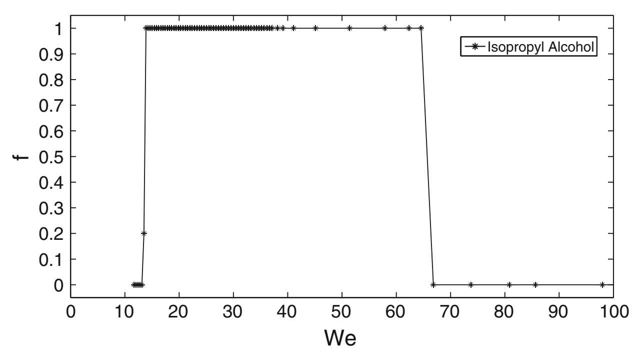


**Fig. 11** Plot of $f$ versus $We$ for isopropyl alcohol

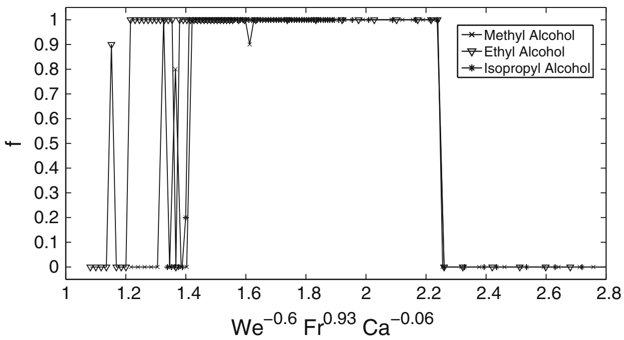


**Fig. 12** Collapse of trailing edges of alcohols data

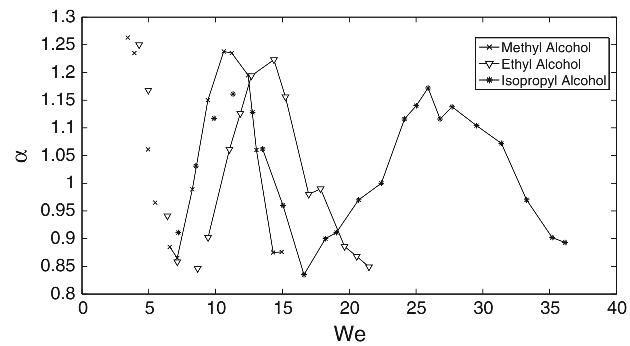


**Fig. 13** Plot of $\alpha$ versus *We* at impact for all three liquids. Data points for which $f = 1$ are connected by a *solid line*

occurrence pattern of all three liquids is nominally digital with an extended Mesler entrainment region ($f = 1$) over the mid-Weber number range. At low *We* where $f = 0$, floating drops were observed. At large *We* where $f = 0$, a single large bubble (and sometimes two large bubbles) was observed. This behavior generally resembles that of the silicone oils tested by Saylor and Bounds (2012). However the methyl alcohol and ethyl alcohol data display different behavior at low *We* where fluctuations in $f$ occur in the form of sharp increases and decreases. This does not occur for isopropyl alcohol. An explanation for this behavior is presented in the "Discussion" section.

Due to the different behavior noted in methyl alcohol and ethyl alcohol at low Weber numbers, the leading edges of the data set could not be uniquely defined, and so we chose to try to collapse the trailing edges of the data sets. The three distinct trailing edges for each of the three alcohols were collapsed using a power law of the form:

$$C = We^{\beta} Fr^{\gamma} Ca^{\delta} \tag{5}$$

where $C$, $\beta$, $\gamma$, and $\delta$ are all (hopefully) constants. As Fig. 12 shows, the scaling $We^{-0.6}Fr^{0.93}Ca^{-0.06}$ successfully collapses the trailing edges of the alcohols investigated in this study with $C = 2.241 \pm 0.001$.

## 4 Discussion

The first goal of this work was motivated by the work of Mills et al. (2012) and Saylor and Bounds (2012). Mills et al. (2012) showed that when water is the working fluid, Mesler entrainment shows highly irreproducible behavior at a fixed *We*, giving a maximum value of $f$ that is less than 0.8 (Fig. 1). Saylor and Bounds (2012) showed that if one uses a silicone oil for the working fluid, the results are highly repeatable, rarely giving a value of $f$ different from zero or unity. The first goal of this research was to determine whether other test liquids are similar to water or to silicone oil. The results presented in Figs. 8, 9, 10 and 11 show that the qualitative behavior of the three alcohols investigated here is much more similar to silicone oil than to water. The present alcohol data give the same repeatability as was observed in silicon oils, the only exception being at low Weber numbers for ethyl alcohol and methyl alcohol. For isopropyl alcohol and for the mid and high Weber number ranges of ethyl and methyl alcohol, $f$ is almost exclusively zero or unity, very similar to that of silicone oil.

The source and significance of the variability in $f$ that is observed at low *We* for methyl and ethyl alcohol and not for isopropyl alcohol is now discussed. One possible explanation for this might be the oscillation in drop shape as the drop falls. Such oscillations are known to occur and to play a role in drop impact phenomena. For example there have been several studies on the effect of the shape of a drop at impact on the formation, speed, and penetration depth of a vortex formed by that impact (Chapman and Critchlow 1967; Durst 1996; Rodriguez and Mesler 1988; Saylor and Grizzard 2003, 2004). Accordingly, we sought to determine whether Mesler entrainment was achieved only for a certain drop shape on impact and whether this might explain the oscillatory values of $f$ at low *We*. To do this, the drop shape at impact was quantified by the axis ratio $\alpha$:

$$\alpha = \frac{d_v}{d_h} \tag{6}$$

where $d_v$ and $d_h$ are the maximum vertical and horizontal extents of the drop just prior to impact with the liquid surface. Hence, an oblate drop has $\alpha < 1$, a prolate drop has $\alpha > 1$, and a spherical drop has $\alpha = 1$. In Fig. 13, $\alpha$ is plotted against *We* for all liquids explored here for the low range of *We*. The data points connected by a line signify values of *We* where $f = 1$ for an extended range. Points where $f \neq 1$ or where the value of $f$ is oscillating with *We* are left unconnected. Data are plotted in Fig. 13 until a complete cycle in drop oscillation occurs over which $f = 1$. What this figure reveals is that Mesler entrainment occurs reproducibly over the entire range of possible drop shapes

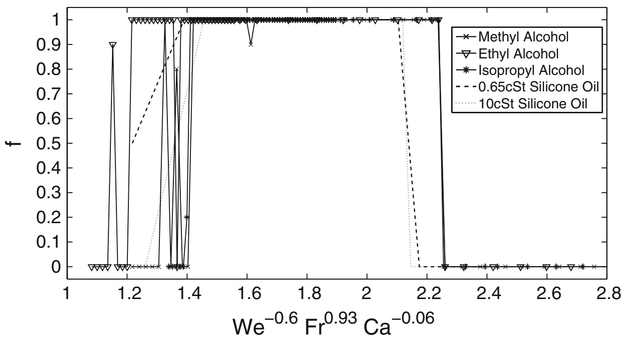


**Fig. 14** Plot of the scaled versions of the alcohol data along with silicone oil data

suggesting that $\alpha$ does not seem to affect Mesler entrainment (at least for the conditions explored in this work). For example, for methyl alcohol, the range where $f = 1$ occurs for $0.85 < \alpha < 1.25$, yet at the same time, at lower *We*, $f$ varies significantly (the data points are not connected) over approximately the same range of $\alpha$. A similar observation can be made for the other two alcohols explored here. Hence, drop shape cannot explain why isopropyl alcohol does not exhibit variability in $f$ at low *We*, while ethyl and methyl alcohol do.

A more likely explanation for the source of variations in $f$ at low *We* for methyl and ethyl alcohol pertains to capillary waves and other secondary oscillations that occur due to the snap-off of the drop from the needle at the moment of release. For ethyl, methyl, and isopropyl alcohol, the values of *We* at which Mesler entrainment is first repeatedly observed are 9.43, 6.57, and 13.9, respectively, which correspond to drop release heights of 10.0 mm, 9.5 mm, and 14.75 mm, respectively. Since the drop release height at which Mesler entrainment is first observed is higher for isopropyl alcohol than the other liquids, there is more time for capillary waves to damp out. Moreover, isopropyl alcohol has a viscosity that is 3.8 times that of methyl alcohol and 1.9 times that of ethyl alcohol, further enabling the damping of those disturbances. The surface tension of isopropyl alcohol is greater than that for the other two alcohols, although only slightly, further enabling a more rapid damping of snap-off disturbances. It seems likely then that disturbances due to needle snap-off dynamics cause the odd behavior of the methyl alcohol and ethyl alcohol data sets in the low *We* range. Accordingly, we conclude that the alcohols explored here are qualitatively similar in behavior to that of silicone oil and that the behavior of water is unusual and likely specific to water.

To determine whether methyl alcohol, ethyl alcohol, and isopropyl alcohol exhibit the same quantitative characteristics as silicone oil (as opposed to the qualitative characteristics discussed above), experiments were also conducted in silicone oils to obtain trailing edge data.

**Table 2** Values of the constant $C$ defined in Eq. (5) for alcohol and silicone oil data sets after scaling

| Liquid | $C$ |
|---|---|
| Methyl alcohol | 2.242 |
| Ethyl alcohol | 2.241 |
| Isopropyl alcohol | 2.239 |
| 0.65 cSt Silicone oil | 2.106 |
| 10 cSt Silicone oil | 2.121 |

These experiments were conducted, as opposed to using the data obtained by Saylor and Bounds (2012), to ensure that all data was acquired using an apparatus of the same spatial resolution. This is important since, as noted earlier, as *We* gets larger, the bubble size gets smaller, indicating that an observation of $f = 0$ could conceivably be due to a simple inability to observe bubbles. The trailing edge silicone oil data presented in this paper were gathered using the strobe-lit experimental setup in Fig. 3. Using this data and the alcohols data already described, the combined data set was scaled according to Eq. (5) and plotted in Fig. 14. This figure shows that the trailing edge of the silicone oil data does not collapse with the alcohols data. In Table 2, the value of $C$, defined in Eq. (5), is presented for the alcohols and silicone oils giving a different value for $C$ for the silicone oils. Additionally, the scaling approach described earlier was repeated, including silicone oil in the data set in an attempt to obtain new values for $\beta$, $\gamma$, and $\delta$ for Eq. (5). However, no values were obtained, our fitting algorithm finding only the trivial solution of $(\beta, \gamma, \delta) \rightarrow 0$.

While the above result is somewhat disappointing, it is also intriguing; the inability to scale our data which is, essentially, five data points, using three-dimensionless groups, suggests that an important piece of physics must be missing. Other researchers have suggested that van der Waals forces may play a role in causing the final collapse of the air film that exists between the liquid drop and the bulk liquid during Mesler entrainment (e.g., Thoroddsen et al. (2012)). This seems unlikely, since van der Waals forces are expected to act over distances comparable to the molecular size, while the air film thickness is estimated to be on the order of 100 nm at collapse. Nevertheless, we developed a dimensionless group which uses the Hamaker constant ($A$), a number that characterizes van der Waals forces on the basis of Lifshitz theory according to the equation (Israelachvili 1992):

$$A = \frac{3}{4}\kappa T\left(\frac{\epsilon_1 - \epsilon_3}{\epsilon_1 + \epsilon_3}\right)^2 + \frac{3h\nu_e}{16\sqrt{2}}\frac{(n_1^2 - n_3^2)^2}{(n_1^2 + n_3^2)^{\frac{3}{2}}} \quad (7)$$

where $\epsilon_1$ and $\epsilon_3$ are the dielectric constants of the liquid and surrounding gas, respectively; $n_1$ and $n_3$ are the indices of refraction for the liquid and surrounding gas,

**Table 3** Values of the Hamaker constant $A$ defined in Eq. (7) for all liquids

| Liquid | $A$ (J) |
|---|---|
| Methyl alcohol | $3.63 \times 10^{-20}$ |
| Ethyl alcohol | $4.23 \times 10^{-20}$ |
| Isopropyl alcohol | $4.56 \times 10^{-20}$ |
| 0.65 cSt Silicone oil | $4.29 \times 10^{-20}$ |
| 10 cSt Silicone oil | $4.81 \times 10^{-20}$ |

respectively, and $\kappa$, $T$, $h$, and $\nu_e$ are the Boltzmann constant, temperature, Planck constant, and the UV electronic absorption frequency, respectively. This equation can be used to calculate the Hamaker constant for a simplified case of two identical fluid surfaces (the drop and liquid) acting along a medium (the surrounding air). The resulting Hamaker constants are compiled for each liquid in Table 3.

The addition of the Hamaker constant ($A$) to the list of relevant variables for bubble formation results in a fourth dimensionless group ($S$).

$$S = \frac{\rho d^3 V^2}{A} \tag{8}$$

Attempts to collapse the trailing edges of the alcohols and silicone oils data sets using a linear combination of $We$, $Ca$, $Fr$, and $S$ also failed. This suggests that the missing piece of physics is not van der Waals forces, but some other phenomenon that has not yet been identified.

Finally, we note that the trailing edge that is presented in the plots of Figs. 8, 9, 10, 11 are not "hard" edges. As $We$ increases, the diameter of the resulting bubbles decreases. Hence, depending on lighting conditions and the spatial resolution of the camera used, it is possible that smaller bubbles are present that simply cannot be observed. Herein, we used a better illumination method and a higher resolution camera for the high $We$ range. However, further improvements in lighting and spatial resolution might reveal Mesler entrainment at yet higher values of $We$ than observed here. This does not, however, change the conclusions of this work, since all of the fluids considered here were studied under the same resolution. It is anticipated that regardless of the spatial resolution of the camera employed in a study of Mesler entrainment, for the fluids tested here, the trailing edge will be sharp, as it is for the plots shown above.

## 5 Conclusion

Mesler entrainment is not reproducible in water, while in silicone oils it has been shown to be reproducible. The goal of this work was to determine whether or not most liquids behave as water does in this regard. Herein, experiments in three alcohols (methyl, ethyl, and isopropyl alcohol) showed reproducible Mesler entrainment for a broad range of Weber number, suggesting that, typically, Mesler entrainment is reproducible and that water is a unique liquid in this regard. Another goal of this work was to determine an appropriate combination of the relevant dimensionless groups that would predict the boundaries where Mesler entrainment exists. We were able to do this using the Weber, Froude, and capillary numbers, but only when just alcohol data were included. When silicone oils were also included in the data set, we were unable to collapse the data. This suggests that some other force or piece of physics needs to be included. Further attempts to collapse our data using a fourth dimensionless group based on the Hamaker constant did not improve the situation, suggesting that van der Waals forces are not the missing piece. Further work is needed to clarify this situation.

## References


Bergman T, Mesler R (1981) Bubble nucleation studies. Part I: Formation of bubble nuclei in superheated water by bursting bubbles. AIChE J 27:851–853

Canny J (1986) A computational approach to edge detection. IEEE Trans Patt Anal Mach Intellig 8:679–698

Carroll K, Mesler R (1981) Part II: Bubble entrainment by drop-formed vortex rings. AIChE J 27:853–855

Chapman DS, Critchlow PR (1967) Formation of vortex rings from falling drops. J Fluid Mech 29:177 – 185

Durst F (1996) Penetration length and diameter development of vortex rings generated by impacting water drops. Exp. Fluids 21:110–117

Esmailizadeh L, Mesler R (1986) Bubble entrainment with drops. J Colloid Interf Sci 110:561–574

Israelachvili JN (1992) Intermolecular and surface forces, 2nd edn. Academic Press, San Diego

Liow JL, Cole DE (2007) Bubble entrapment mechanisms during the impact of a water drop. In: 16th Australasian fluid mechanics conference, pp 866–869. Gold Coast, Australia

Mesler R (1976) A mechanism supported by extensive experimental evidence to explain high heat fluxes observed during nucleate boiling. AIChE J 22:246–252

Mesler R, Mailen G (1977) Nucleate boiling in thin liquid films. AIChE J 23:954–957

Mills BH, Saylor JR, Testik FY (2012) An experimental study of Mesler entrainment on a surfactant-covered interface: the effect of drop shape and Weber number. AIChE J 58:46–58

Oğuz HN, Prosperetti A (1989) Surface-tension effects in the contact of liquid surfaces. J Fluid Mech 203:149–171

Pumphrey HC, Elmore PA (1990) The entrainment of bubbles by drop impacts. J Fluid Mech 220:539–567

Rodriguez F, Mesler R (1988) The penetration of drop-formed vortex rings into pools of liquid. J Coll Interf Sci121:121–129

Saylor JR, Bounds GD (2012) Experimental study of the role of the Weber and capillary numbers on Mesler entrainment. AIChE J 58:3841–3851

Saylor JR, Grizzard NK (2003) The effect of surfactant monolayers on vortex rings formed from an impacting water drop. Phys Fluids 15:2852–2863

Saylor JR, Grizzard NK (2004) The optimal drop shape for vortices generated by drop impacts: the effect of surfactants on the drop surface. Exp Fluids 36:783–790

Sigler J, Mesler R (1990) The behavior of the gas film formed upon drop impact with a liquid surface. J Coll Interf Sci 134:459–474

Thoroddsen ST, Etoh TG, Takehara K (2003) Air entrapment under an impacting drop. J Fluid Mech 478:125–134

Thoroddsen ST, Thoraval MJ, Takehara K, Etoh, TG (2012) Micro-bubble morphologies following drop impacts onto a pool surface. J Fluid Mech 708:469–479

Weast RC (2012) Handbook of chemistry and physics, 92 edn. Chemical Rubber Company, Cleveland